Structural Insight into Geranylgeranyl Diphosphate Synthase (GGDPS) for Cancer Therapy

Andrew C. Pham[1], Sarah A. Holstein[2], and Gloria E.O. Borgstahl[1,3]

ABSTRACT

Geranylgeranyl diphosphate synthase (GGDPS), the source of the isoprenoid donor in protein geranylgeranylation reactions, has become an attractive target for anticancer therapy due to the reliance of cancers on geranylgeranylated proteins. Current GGDPS inhibitor development focuses on optimizing the drug-target enzyme interactions of nitrogen-containing bisphosphonate-based drugs. To advance GGDPS inhibitor development, understanding the enzyme structure, active site, and ligand/product interactions is essential. Here we provide a comprehensive structure-focused review of GGDPS. We reviewed available yeast and human GGDPS structures and then used AlphaFold modeling to complete unsolved structural aspects of these models. We delineate the elements of higher-order structure formation, product-substrate binding, the electrostatic surface, and small-molecule inhibitor binding. With the rise of structure-based drug design, the information provided here will serve as a valuable tool for rationally optimizing inhibitor selectivity and effectiveness.

Introduction

Protein geranylgeranylation is a posttranslational modification critical for the proper localization and function of certain classes of membrane-associated proteins. Geranylgeranylation involves the attachment of one or two 20-carbon isoprenoid groups (geranylgeranyl chains) to cysteine residues near the C-terminus of a CaaX or CaaX-like motif (C is cysteine, a is an aliphatic amino acid, and X is any other amino acid; ref. 1). Adding the hydrophobic geranylgeranyl chains allows proteins to be targeted and anchored in cell or organelle membranes. The most commonly geranylgeranylated proteins include those belonging to families within the Ras superfamily of small GTPases, which play essential roles in cancer progression (2–4). These geranylgeranylated proteins are involved in numerous downstream processes, including cell division, differentiation, metabolism, cellular trafficking, and chemokine signaling (5–7). Recent studies also have identified FBXL2 (ubiquitin ligase subunit) and Ykt6 (V-SNARE homolog) to be geranylgeranylated (8, 9).

Geranylgeranyl diphosphate synthase (GGDPS), an enzyme that is a part of the mammalian isoprenoid biosynthetic pathway, catalyzes the synthesis of geranylgeranyl diphosphate groups (GGDP). Synthesis occurs through a condensation reaction involving two isoprenoid substrates, farnesyl diphosphate (FDP, 15 carbons long) and isopentenyl pyrophosphate (IPP, 5 carbons long). GGDP is the isoprenoid donor for protein geranylgeranylation reactions and the precursor for vitamin K2 and ubiquinone synthesis. Depending on the target protein, one of three different geranylgeranyl transferase (GGTase) enzymes will catalyze the transfer reaction (10). Proteins in the Rho family of GTPases (i.e., RhoA) are geranylgeranylated by GGTase-I. GGTase-II (also known as RabGGTase) geranylgeranylates proteins in the Rab family (11, 12). The newly discovered GGTase-III modifies non-GTPase substrates such as FBXL2 and Ykt6 (13). The identity of amino acids encompassing the C-terminal cysteine residue dictates substrate specificity (14).

There is interest in GGDPS as a therapeutic target in cancer, given the roles of geranylgeranylated proteins in regulating cancer cell proliferation/survival, migration/invasion, and intracellular transport (15–18). Ongoing research continues to uncover new links between geranylgeranylated proteins and disease progression. While not covered in this review, dysregulation of GGDPS expression and/or activity also has important links to the pathophysiology of Alzheimer disease, type 2 diabetes, liver disease and pulmonary disease. The putative mechanisms underlying these links were recently reviewed by Muehlebach and Holstein (15). Thus, the development of GGDPS inhibitors represents a burgeoning field in drug discovery and development.

Structure-guided drug design has become increasingly popular as it is more efficient and economical (19). As the current landscape of structural techniques evolves, the reliability of structure-based drug design continues to improve (20). For GGDPS, a significant challenge is the lack of structures published in the protein data bank (PDB) and no single resource to compare structural findings. Deposited crystal structures vary both in species and bound ligands. This review aims to provide a comprehensive overview of the human (hGGDPS) and yeast (yGGDPS) structures to serve as a "one-stop-shop" for information relating to GGDPS structure. This will include an analysis of the interfaces responsible for oligomerization, a rigorous evaluation of the substrate/product-binding site, an examination of the electrostatic protein surface, and an overview of inhibitor-bound structures.

Cancer Relevance

Multiple studies have demonstrated that GGDPS inhibition results in anti-proliferative effects in cancer cells due to protein geranylgeranylation disruption (21–26). Effects on autophagic flux, migration, and invasion have also been reported (21, 27–29). As GGDPS inhibition results in global disruption of protein geranylgeranylation, there

[1]Department of Biochemistry and Molecular Biology, University of Nebraska Medical Center, Omaha, Nebraska. [2]Department of Internal Medicine, University of Nebraska Medical Center, Omaha, Nebraska. [3]The Eppley Institute for Research in Cancer and Allied Diseases, University of Nebraska Medical Center, Omaha, Nebraska.

Corresponding Author: Gloria E.O. Borgstahl, The Eppley Institute for Research in Cancer and Allied Diseases, University of Nebraska Medical Center, 986805 Nebraska Medical Center, Omaha, NE 68198. E-mail: gborgstahl@unmc.edu

Mol Cancer Ther 2024;23:14–23

doi: 10.1158/1535-7163.MCT-23-0358

has been interest in determining whether the observed effects on malignant cells are secondary to a particular subset of geranylgeranylated proteins. As recently reviewed, the relative importance of disrupting GGTase-I versus GGTase-II substrate geranylgeranylation varies amongst malignancies (15). While initially there was a greater focus on the impact of GGTase-I inhibition, primarily as a means to target oncogenic K-Ras as well as Rho and Rac family members (30), more recent work has indicated that disruption of Rab geranylgeranylation is a key mechanism underlying the efficacy of GGDPS inhibitors in several malignancies characterized by abnormal protein production.

Work done in multiple myeloma revealed that GGDPS inhibition results in the induction of the unfolded protein response pathway (UPR) via disruption of monoclonal protein trafficking. As myeloma cells are highly secretory, they are sensitive to therapies that disrupt protein homeostasis (31). GGDPS inhibition results in the accumulation of monoclonal protein within the endoplasmic reticulum (ER), leading to ER stress, activation of the UPR, and, ultimately, apoptosis (32–34). Through the use of specific GGTase-I and GGTase-II inhibitors, it was found that disruption of Rab geranylgeranylation was the major mechanism of GGDPS inhibitors (32). Similarly, in work done in pancreatic ductal adenocarcinoma (PDAC), GGPDS inhibition disrupted mucin trafficking and caused induction of the UPR and apoptosis, all via the disruption of Rab geranylgeranylation (35). That these effects do not require complete cessation of protein trafficking are consistent with the higher dependency of malignant cells on geranylgeranylated proteins and intact protein homeostasis pathways compared with normal cells, thus providing a therapeutic window. Interestingly, while neither osteosarcoma nor Ewing sarcoma are highly secretory malignancies, recent work demonstrated that the effects of GGDPS inhibition in inducing the UPR and apoptosis were secondary to disruption of Rab geranylgeranylation (29). *In vivo*, GGDPS inhibitors were effective in mouse models of prostate cancer, multiple myeloma, PDAC, and Ewing sarcoma (29, 34–40).

Several studies have shown a correlation between increased GGDPS expression and cancer progression. One study observed overexpression of GGDPS in lung adenocarcinoma (41). This upregulation was associated with increased tumor size, lymph node metastasis, and poor prognosis. GGDPS knockdown caused diminished invasion and migration of lung adenocarcinoma cells. Another study discovered increased GGDPS gene and protein expression in hepatocellular carcinoma tissues and patients with cirrhosis (42). Increased GGDPS expression was associated with several pathologic characteristics such as tumor stage, vessel invasion, and early recurrence.

Thus, while GGDPS is not yet a clinically validated target, substantial data demonstrate this enzyme's relevance in malignancy and support the further development of GGDPS inhibitors. As described below, the existing structure–activity relationships (SAR) reported to date have highlighted the complexity of the inhibitor–enzyme–substrates–product interactions. Further understanding of the structural biology aspects of GGDPS and these interactions will provide insight into the observed SARs and guide the design of next-generation inhibitors. In the following sections, we will explore what is known about GGDPS structure and function.

Structural Overview

Higher-order organization of GGDPS subunits

Scientists have debated the quaternary structure of GGDPS, even up to today. GGDPS was first partially purified in 1992 by Sagami and coworkers from pig liver (43). They observed a molecular mass of 300 kDa with a monomer mass of 120 kDa. Two years later, the same group purified GGDPS from bovine brain (44). This time, they observed GGDPS as a homo-oligomer (150–195 kDa) with an apparent monomer molecular weight of 37.5 kDa, suggesting either a tetrameric or pentameric form. They concluded that GGDPS "occurs in a complex form composed of several different or complex subunits". Early structures of yGGDPS revealed the protein to be dimeric (PBD: 2DH4; ref. 45). This finding was shared in archaeal (PDB: 1WY0) and bacterial species (PDB: 1WMW). The high sequence similarity between hGGDPS and yGGDPS suggested that hGGDPS could also exist as a dimer (46). In 2006, Kavanaugh and coworkers solved the first hGGDPS crystal structure, revealing the human enzyme to be a hexamer (47). A "3-bladed propeller arrangement" was seen where each monomer associates with one other identical monomer to form a dimer. In addition, each monomer interacts with two more chains to form a trimer-like structure. A dimer of these trimers forms the hexameric structure.

Lower-level species seem to exhibit the dimeric form of GGDPS. Bacterial, parasite, and even plant GGDPS all share this dimeric organization (48–50). Some plant and bacterial species even have tetrameric forms of GGDPS (51), contributing to the pool of GGDPS oligomerization states. A recently published structure from a bacterial species showed the hexameric form, similar to hGGDPS (PDB: 6KD7; ref. 52). Miyagi and coworkers have reported an active 280-kDa octamer form of hGGDPS (53), which could convert into dimeric or hexameric states when reduced (54). With this knowledge, the debate persists regarding the active form of hGGDPS. As the dimeric and hexameric states have supporting structural data in hGGDPS, we will describe the key residues and interfaces involved.

Dimeric interface

The dimeric organization of GGDPS is seen across multiple species. In humans, a similar dimeric interface occurs with the overall quaternary structure referred to as a "trimer of dimers" (40). In the hGGDPS crystal structure, dimers form between chains A and B (green and cyan), C and D (yellow and magenta), as well as E and F (salmon and gray). The dimeric interface can be seen between chains A and B in Supplementary Fig. S1A. These chains will be referred to by the colors shown in the figures as described above from now on. The PyMOL *InterfaceResidue* script was used to illustrate the residues involved at the dimeric hGGDPS interface (55). As the dimeric interface is extensive, rather than focusing on the contributions of each individual residue, we focused on the contributions of each helix. The interface is composed of amino acid residues involved in electrostatic, Van der Waals, and hydrogen bonding interactions. Most of the contacts at the dimer interface are between helix α4 and helix α5. The interactions between helix α4 and helix α5 alone contribute an area of 4699.92 $Å^2$. Given the entire interface spans an area of 8597.46 $Å^2$, the helix α4 and α5 contact comprise over 50% of the dimer interface. Helix α1 also contributes to the dimer interface as it forms interactions with helices α5 and α6 of the opposing chain. In addition, helix α3 forms interactions with helix α4. A list of the specific residues involved in the dimeric interface is given (Supplementary Table S1).

Trimeric interface

In hGGDPS, the dimers trimerize to form a hexamer. The trimeric interface (called the "inter-dimer" interface by Kavanaugh and colleagues), which is responsible for forming the trimer of dimers, spans a total of 2631.10 $Å^2$ (Supplementary Fig. S1B). On one side of the hexamer, the trimeric interfaces form between the green, salmon, and

yellow chains. On the opposite end, it forms between the cyan, magenta, and gray chains. When focusing on a single GGDPS monomer (green) and its associated trimeric partners (salmon and yellow), two regions are observed. Region 1 (maroon) includes residues from helices α1 and α4. Region 1 of the green chain interacts with region 2 (sky blue) of the adjacent salmon chain. Region 2 includes residues from helices α9 and α10. Likewise, the green chain will contain a region 2, which interfaces with region 1 of the adjacent yellow chain, and the yellow chain will contain a region 2, which interfaces with region 1 of the adjacent salmon chain. This effectively creates a stable network between the three chains where each chain is seen to interact with both sets of partners through the same set of residues. The same contacts and interfaces are observed between the cyan, magenta, and gray chains on the opposite side. The residues involved at this interface are listed in Supplementary Table S1 categorized by their region.

The hexameric organization of hGGDPS can be disrupted by making a single Y246D point mutation (40). When Lacbay and coworkers made this mutation, they observed the hexameric hGGDPS crystallized as a dimer. It was stated to be more readily crystallizable but still retained the same overall structure and catalytic activity. Tyr246 is in the center of region 2 and stabilizes pi-bond interactions with Phe76 and Tyr18 of the neighboring chain. In addition, Tyr246 acts as a hydrogen bond donor to Gln21 (distance of 3.5 Å). The Y246D mutation abrogates the hydrophobic pi-stacking seen between Phe76 and Tyr18. With the Y246D mutation, the formation of the hexamer would bury a negative charge in the trimeric interface without charge compensation, energetically a highly unfavorable situation.

Given the importance of quaternary structure in stabilizing hGGDPS, it is reasonable to assume that disrupting the dimeric or trimeric interfaces could hinder GGDPS activity. With the knowledge available for both interfaces, designing peptides or small molecules targeting oligomerization could be an effective strategy. Evidence exists for multiple possible oligomerization states, but whether the quaternary structure is related to overall function is unknown. Miyagi and coworkers found that hGGDPS could be converted to a dimer or hexamer from an octamer with a reducing agent, suggesting potentially different roles for each form in different environments, but further studies are warranted (54).

Yeast and human sequence and structure alignment

Understanding how the isoprene substrates and product bind the active site is critical in predicting GGDPS inhibitor binding. Unfortunately, hGGDPS structures in the PDB are limited and of moderate resolution (2.2 Å–3.5 Å). In addition, there are no substrate-bound hGGDPS structures and only one product-bound structure. Even in the highest resolved structure of hGGDPS (PDB: 6R4V), residues from the N-terminus (Met1 – Gln5), a loop (Lys196 – Asn201), and C-terminus (Glu297 – Glu300) are missing (56). These regions are consistently unresolved across published structures suggesting high disorder or flexibility. To portray a more complete analysis of the protein surface, AlphaFold (57) was used to model these regions (Supplementary Fig. S2A). From this section forward, $hGGDPS^{AF}$ or AF 2Q80 will refer to the AlphaFold-corrected human protein. While the $hGGDPS^{AF}$ model is used for the rest of the paper, it provides the most value in the electrostatic surface section. In the case of discerning the binding sites and oligomeric interfaces, these residues are well characterized with supporting crystal structure data.

While there are no published substrate-bound hGGDPS structures, a yeast structure with both substrates in the binding site does exist (PDB: 2E8T; ref. 46). We wondered if the substrate-bound yGGDPS structure gave an accurate representation of the substrate-binding site in hGGDPS, so we performed an alignment of the hGGDPS (UniProt: O95749) and yGGDPS (UniProt: Q12051) sequences using JalView (58). Overall, the amino acid properties are well conserved between yeast and human GGDPS (Supplementary Fig. S2B), with 39.2% being identical in amino acid and position (Supplementary Fig. S2C). Most of the protein is composed of α-helices, and regions that are conserved in amino acid identity were also identical in secondary structure (see the overlaid panels in **Figs. 1** and **2**). These regions correspond to residues involved in substrate/product binding. Given the structural and sequence similarity between the two enzymes, the binding pockets appear to be conserved between species. The structure of the GGDPS binding sites, along with the interacting amino acids of the two major substrates and product, will be further elaborated below.

Substrate Binding

IPP (site 1)

IPP is the first of two substrates for GGDP formation. IPP is the smallest GGDPS substrate, containing only a 5-carbon chain. IPP is the "building block" for the rest of the isoprenoids. The IPP binding pocket was characterized in yGGDPS by Guo and coworkers (46). As previously stated, there are no solved structures of IPP-bound hGGDPS, so a model for human IPP binding was calculated by superimposing $hGGDPS^{AF}$ with FDP-IPP-bound yGGDPS (PDB: 2E8T). The corresponding human GGDPS residues involved in IPP binding are shown both superimposed and individually in **Fig. 1A**. See Supplementary Table S2 for a list of yeast and human IPP binding residues. Guo and coworkers showed that IPP could occupy two distinct sites depending on substrate availability, naming them the homoallylic and allylic sites. The homoallylic site is the primary IPP binding site and is similar to the IPP binding site in the highly related farnesyl diphosphate synthase (FDPS) enzyme (59). Residues implicated in IPP binding are almost completely conserved between species, with the only difference being a tyrosine residue in yeast (Tyr205) versus a phenylalanine in human (Phe184). Even then, the aromaticity of the binding pocket is conserved between the two species. This aromatic ring may be responsible for stabilizing the IPP isoprene tail, as the short chain of IPP requires fewer interactions to stabilize binding. Positively charged arginine and histidine residues stabilize the negatively charged phosphate heads of IPP (yGGDPS: Arg39, His68, and Arg85; hGGDPS: Arg28, His57, and Arg74). Of note, Arg28 points away from the diphosphate moiety in the human structure, while the complimentary Arg39 in yeast faces toward it. This difference is likely because the $hGGDPS^{AF}$ structure contains nothing bound at this site. At the homoallylic site, IPP diphosphate does not interact with Mg^{2+}. Instead, longer chained substrates (such as FDP) simultaneously occupying the active site will have their phosphate heads occupying regions near Mg^{2+}. When IPP is the only substrate present, IPP can occupy both the homoallylic and allylic sites due to its short isoprene side chain. Classically, the allylic site is where the FDP substrate binds. When IPP is bound to both homoallylic and allylic sites, IPP can chelate to Mg^{2+}.

FDP (site 2)

FDP is the second canonical GGDPS substrate. FDP contains a 15-carbon tail and a diphosphate group. Guo and coworkers revealed the FDP binding site in yeast GGDPS (46). They noticed that the longer FDP group occupied a different site than IPP. As before, we built a model for FDP binding to $hGGDPS^{AF}$ by overlaying human and yeast enzymes (**Fig. 1B**). A list of residues

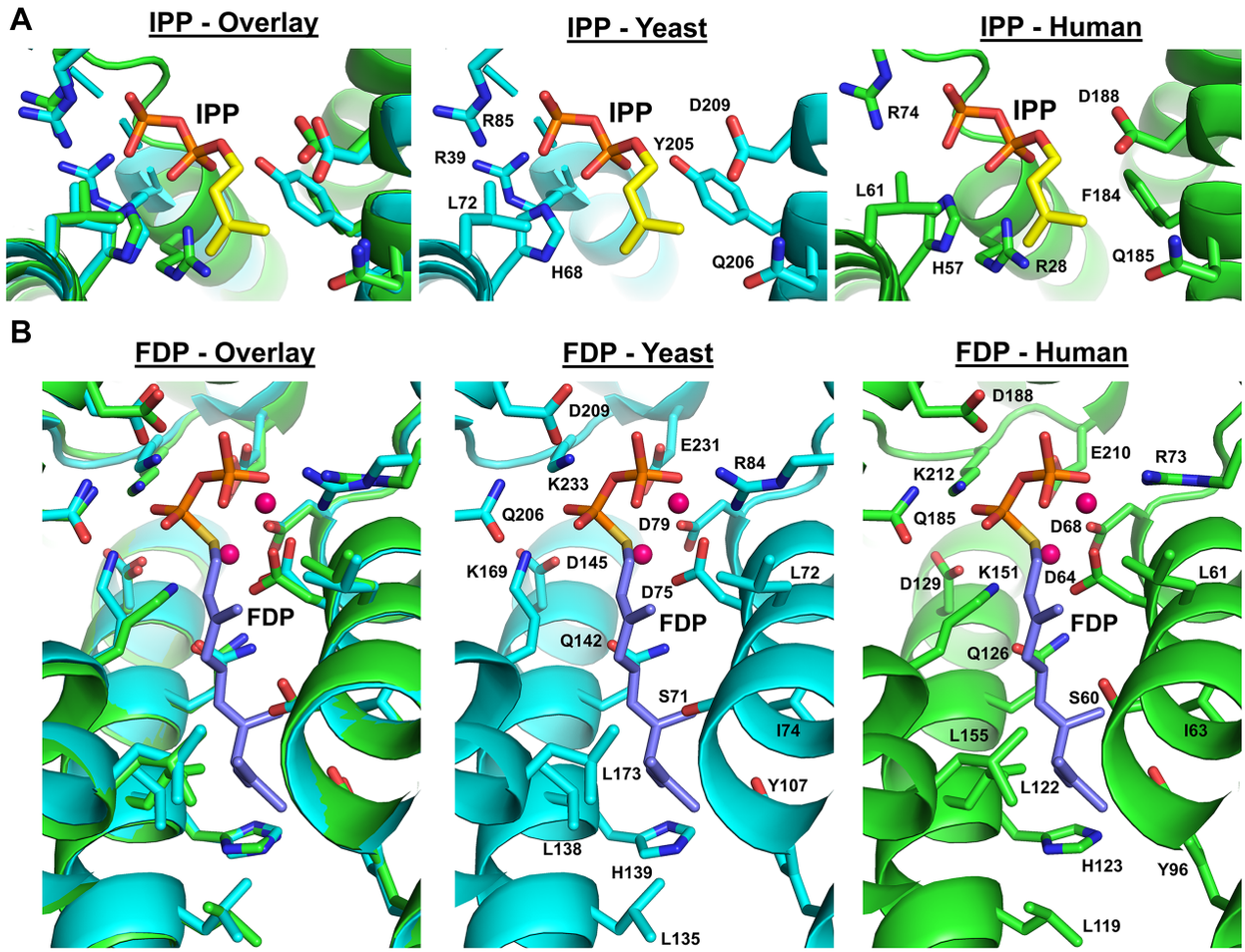

Figure 1.

The substrate binding sites (IPP and FDP). Residues found within 4 Å of the GGDPS substrates in yeast (cyan) and human (green) are represented as sticks. The human AF 2Q80 and IPP-FDP bound yGGDPS structures were used (PDB: 2E8T). **A,** The IPP binding site (site 1). hGGDPS^{AF} overlaid on top of the IPP-FDP bound yGGDPS shows amino acid residues within 4 Å of the IPP substrate are highly conserved. Individual residues for yGGDPS IPP binding and the corresponding hGGDPS^{AF} IPP binding sites are shown in the following columns. **B,** The FDP binding site (site 2). hGGDPS^{AF} overlaid on top of the IPP-FDP bound yGGDPS shows amino acid residues within 4 Å of the FDP substrate are highly conserved. Individual residues for yGGDPS FDP binding and the corresponding hGGDPS^{AF} FDP binding sites are shown in the following columns. Mg^{2+} ions are represented as magenta spheres with positions taken from the hGGDPS^{AF} structure.

involved in yeast and human FDP binding is in Supplementary Table S2.

The diphosphate head of FDP interacts with Mg^{2+} and positively charged arginine and lysine residues. Within this binding pocket, a set of negatively charged aspartate and glutamate residues function to ligate the Mg^{2+} at the binding site. Given the highly negative charge of the lipophilic FDP substrate, it is reasonable that both Mg^{2+} and the positive residues play roles in stabilizing the diphosphate group. The GGDPS enzyme also contains several aspartate motifs conserved between all species that are found at this binding site (47). Asp75 and Asp79 (in humans, Asp64 and Asp68) are part of a highly conserved DDIED motif. Asp209 in yeast and Asp188 in humans are part of a highly conserved DDYXN motif. These motifs are likely essential in substrate binding as they play roles in chelating the imperative Mg^{2+} ions at the active site. Implicated FDP binding residues are completely conserved between human and yeast GGDPS in amino acid identity, position, and secondary structure. The isoprene chain of FDP lies within a hydrophobic channel composed of leucine and isoleucine residues. Historically, competitive inhibitors which inhabit the substrate-binding pockets have remained a common mechanism of inhibition (60, 61).

Reaction Mechanism and Product Binding

Reaction mechanism

Geranylgeranyl diphosphate (GGDP) is the 20-carbon product of GGDPS. The reaction mechanism proceeds through an ionization-condensation-elimination reaction similar to FDPS (62, 63). When enzyme-bound, FDP undergoes cleavage at the C-1-O bond. The result is a carbocation intermediate stabilized by the negatively charged diphosphate and the highly conserved KT motif at the active site (yGGDPS: Lys169 and Thr170; hGGDPS: Lys151 and Thr152).

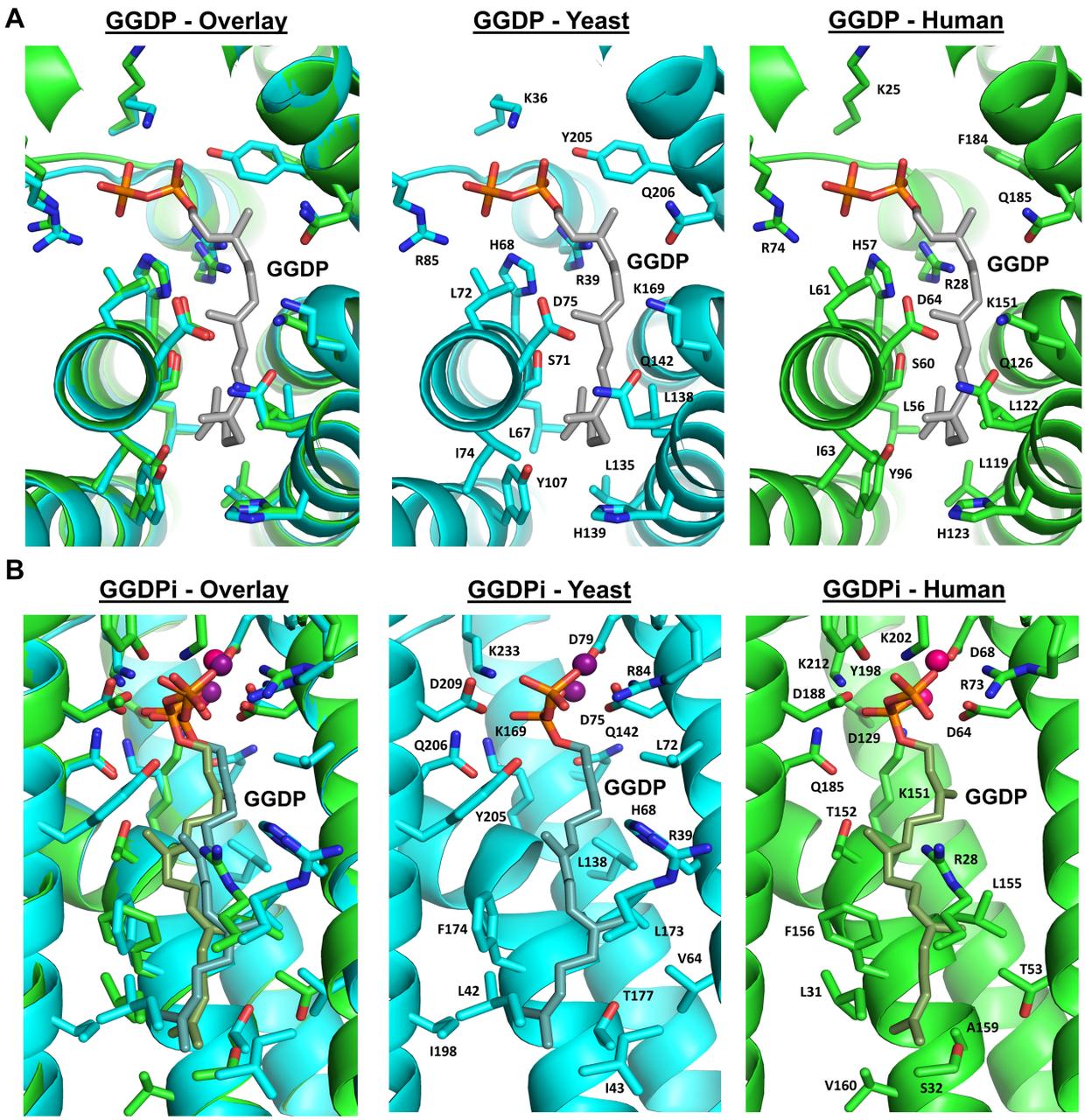

Figure 2.

The product-binding sites (GGDP and GGDPi). The GGDP binding site (site 3). Residues found within 4 Å of the GGDPS product in its classical and inhibitory site in yeast (cyan) and human (green) are represented as sticks. The human AF 2Q80 and GGDP bound yGGDPS structures were used (PDB: 2E8V and 2Z4V). **A,** The classical GGDP binding site (site 3). hGGDPS^{AF} overlaid on top of the classically GGDP bound yGGDPS shows amino acid residues within 4 Å of the GGDP product are highly conserved. Individual residues for yGGDPS classical GGDP binding and the corresponding hGGDPS^{AF} GGDP binding sites are shown in the following columns. **B,** The GGDP inhibitory (GGDPi) binding site (site 4). hGGDPS^{AF} bound at the inhibitory GGDP site overlaid on top of the inhibitory GGDP bound yGGDPS. 18/24 (75%) of the residues found to be within 4 Å of the GGDPi product in either yGGDPS or hGGDPS were completely conserved suggesting high conservation of product-binding residues. Individual residues for GGDPi yGGDPS and GGDPi hGGDPS binding are shown in the following columns. Mg^{2+} ions are represented as purple spheres in the yGGDPS structure and as magenta spheres in the hGGDPS^{AF} structure.

Condensation occurs between the first carbocation intermediate with IPP, resulting in a second positively charged carbocation intermediate. Finally, a stereospecific elimination of a proton results in the final GGDP product (47).

Product binding

Published structures have elucidated two product-binding sites (Supplementary Table S3). One is the "classical" site (**Fig. 2A**), and the other is the "inhibitory" site (**Fig. 2B**). We will first discuss the classical product site. Similar to the substrate binding sites, only a yeast structure with the product bound at the classical site exists. In this mode, GGDP overlaps with the FDP and IPP binding sites (**Fig. 3A**). The product diphosphate group occupies the same space as the IPP diphosphate group. The GGDP isoprene chain interacts with similar leucine and isoleucine as FDP isoprene binding. Found near the FDP binding site are three residues: Leu67, Tyr107, and His139, which serve as a "cap" to prevent chain elongation (46). This is why the GGDP isoprene side chain bends slightly into the IPP isoprene binding site. The highly conserved KT motif thought to stabilize the carbocation intermediates during catalysis is also observed near the product-binding pocket (yGGDPS: Lys169 and Thr170; hGGDPS: Lys151 and Thr152).

Unlike the other binding sites, a structure with the GGDP product bound at the inhibitory site (GGDPi) has been solved for both yeast and human (**Fig. 2B**) (PDB: 2Z4V and 2Q80, respectively). The general position of the GGDP product is the same in both structures, and many of the interacting amino acids are the same. The slight differences in amino acids within 4 Å of the GGDPi site could be due to the differences in resolved structure resolution (1.86 Å in the yGGDPS structure and 2.70 Å in the hGGDPS structure). Between both structures, a total of 24 amino acids are implicated in GGDPi binding, with 75% of the amino acids being completely conserved in identity (Supplementary Table S3). At the GGDP inhibitory site, the GGDP diphosphate head occupies the same site as the FDP diphosphate head, but its isoprene chain occupies a distinct ∼25 Å long hydrophobic channel composed of leucine, isoleucine, and valine residues.

Structurally, it appears that GGDP binding can mimic substrate binding as many of the interacting residues overlap between the two. GGDP can also occupy a distinct "inhibitor" site, which appears to be involved with negative feedback. In fact, GGDP can competitively inhibit both FDP synthesis and its own synthesis (44, 64), supporting regulatory roles based on which binding site GGDP occupies.

Electrostatics of Substrate Binding

The electrostatic surface of GGDPS plays a significant role in the binding of substrates and stabilization of the product (Supplementary Fig. S3). Mg^{2+} ions coordinate with the substrates in the active site. The exact number of Mg^{2+} ions at the active site remains debated, with crystal structures containing 0 to 3 Mg^{2+} ions. These differences are likely due to differences in the crystallization conditions (e.g., pH) and resolution of the crystallographic data. While most structures contain two Mg^{2+} ions at the active site (46, 47), Lisnyanksy and coworkers found three Mg^{2+} ions in their 2.2 Å ibandronate-bound hGGDPS

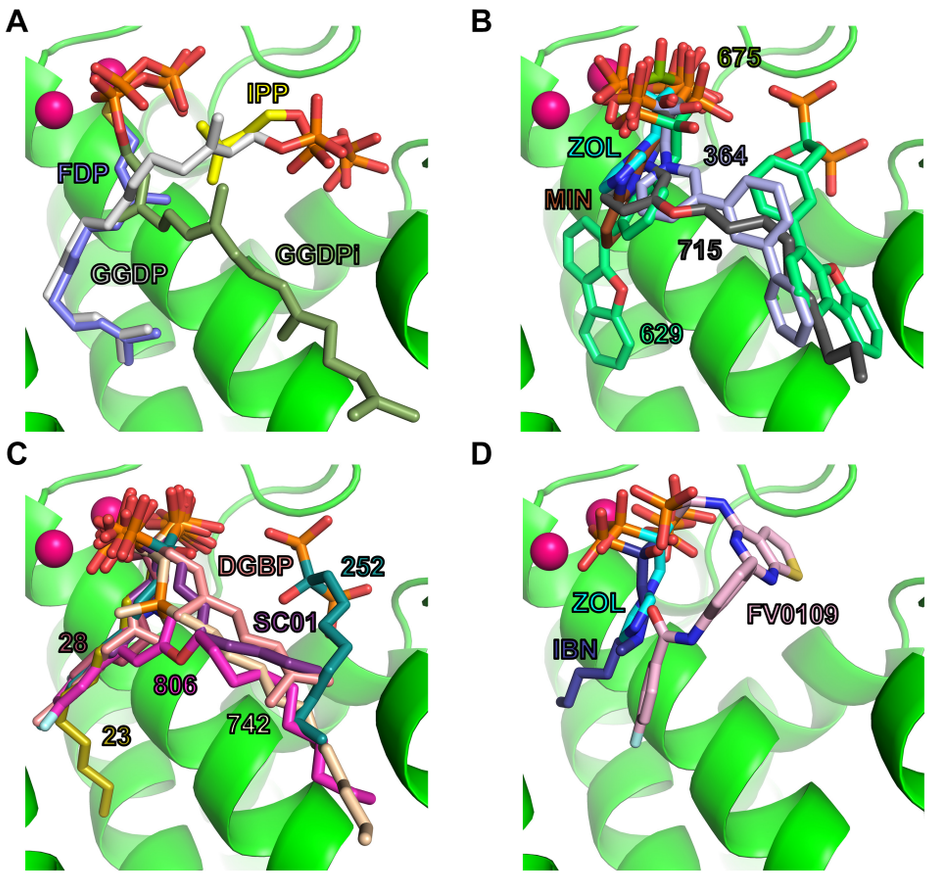

Figure 3.
Overlay of published ligand-bound GGDPS structures in the hGGDPS^{AF} active site. **A,** Overlay of the substrates (IPP and FDP) and product (both GGDP and GGDPi sites). **B,** Overlay of the yGGDPS structure compounds from Chen / Zhang and colleagues in the hGGDPS active site. PDB codes and color are as follows: 2E91 (cyan), 2E92 (brown), 2E93 (sea foam green), 2E94 (light blue), 2E95 (forest green), 2ZEU (dark gray). Bisphosphonate compounds are labeled on the basis of their numbers used in the text. Zoledronic acid (ZOL) and minodronate (MIN) are also abbreviated in the figure. **C,** Overlay of the compounds coming from Guo and colleagues. PDB codes and colors: 2Z4W (salmon), 2Z4Y (teal), 2Z4Z (purple), 2Z50 (brick red), 2Z52 (gold), 2Z7I (tan), 2Z78 (magenta). Structures were solved with the yGGDPS enzyme and overlaid onto the hGGDPSAF active site. Bisphosphonate compounds are labeled on the basis of the number and abbreviations used in the text (DGBP). **D,** Overlay of compounds from solved drug-bound hGGDPS structures. FV0109 is the thienopyrimidine-based bisphosphonate investigated by Lacbay and coworkers (PDB: 6C57, pink). Structures of zoledronate (ZOL) and ibandronate (IBN) were solved by Lisnyansky and colleagues. PDB codes are: 6G31 (cyan), 6R4V (dark blue).

structure (PDB: 6R4V; ref. 56). In addition to the already established Mg^{2+} binding sites (those coordinated with human residues Asp64 and Asp68), they found an additional Mg^{2+} binding site coordinated with Asp188 to be vital for drug binding. For this review, we calculated the electrostatic surface of GGDPS with two Mg^{2+} ions at the active site (those which ligate to Asp64 and Asp68 in human; Asp75 and Asp79 in yeast) as most solved structures only assign these two Mg^{2+} ions. Without Mg^{2+} coordination, the electrostatic surface of the protein is rather neutral (Supplementary Fig. S3A). When Mg^{2+} is bound at the active site, it creates a more positively charged protein surface (Supplementary Fig. S3B). Aside from stabilization of the negatively charged phosphate heads of the lipophilic ligands, this positive surface could also draw in these lipophilic substrates. Whether Mg^{2+} binds the active site prior to substrate-binding is unknown, with conflicting results from apo GGDPS structures. A 1.98 Å apo structure of yGGDPS (PDB: 2DH4; ref. 45) shows Mg^{2+} at the active site, while a 2.80 Å apo structure of the dimeric hGGDPS mutant (PDB: 6C56) and a 3.28 Å apo structure of $hGGDPS^{D188Y}$ (PDB: 6G32) both show no Mg^{2+} at the active site (40, 65). This, again, could be a result of resolution differences, but further confirmation is warranted.

Inhibitor Binding

The majority of reported GGDPS inhibitors contain a bisphosphonate group, similar to the clinically used FDPS inhibitors (e.g., zoledronic acid). Thus, drug development targeting GGDPS began with the knowledge that bisphosphonate served as an important pharmacophore. Even though there is a limited amount of solved eukaryotic GGDPS structures, many deposited structures are bisphosphonate-bound. While most of these structures are of yGGDPS, drug-bound hGGDPS structures have also been published. A summary of the PDB codes and compound names of the drug-bound yGGDPS and hGGDPS structures are displayed in Supplementary Table S4. The structures of the discussed compounds, along with their IC_{50} or EC_{50} values, are shown in Supplementary Table S5. These drug-bound structures will be summarized in this section along with their SAR according to the group which published them.

In 2007 Guo and coworkers solved five inhibitor-bound yGGDPS structures (46). They reasoned that adding more hydrophobic features to zoledronic acid could improve binding to GGDPS. This would not only increase hydrophobic stabilization but also enhance lipophilicity in cells. Their product and substrate-bound yGGDPS structures showed clear possible binding modes for bisphosphonates. The bisphosphonate moieties bind at either the IPP or FDP diphosphate sites. The hydrophobic side chains can bind in the FDP site, the IPP site (for small isoprene chains), or the inhibitory GGDP site (**Fig. 3A**).

The yGGDPS structures containing the FDPS inhibitors zoledronic acid and minodronate (PDB: 2E91 and 2E92) showed the bisphosphonate backbones interacting with Arg84, Lys169, Asp209, and Lys223 via hydrogen bonds. These structures illustrated the importance of the Mg^{2+} as the bisphosphonates formed GGDPS complexes containing two Mg^{2+} coordinated to the conserved aspartate residues. In addition, the imidazole group in zoledronic acid could hydrogen bond to the sidechain oxygen of Thr170 and the main chain carbonyl oxygen of Lys169. These residues are implicated in catalysis, suggesting an important role for nitrogen-containing rings in inhibitors. Results from these solved structures of GGDPS bound by FDPS inhibitors revealed initial structure–activity relationships. Although, it is worth noting these inhibitors only weakly inhibited GGDPS. Therefore, there was still much information needed to decipher the pharmacological blueprint for selective GGDPS inhibition.

Guo and coworkers then examined the binding of three more potent GGDPS inhibitors: BPH-364, BPH-629, and BPH-675. In BPH-364 and BPH-675, they observed binding at the FDP-GGDPi site. The bisphosphate groups bind at the FDP diphosphate site and chelate to Mg^{2+}. The isoprene side chains occupied the channel found in the GGDPi site as both drugs contained large hydrophobic moieties. However, in the case of BPH-629, they observed two binding sites. In the first mode, BPH-629 binds similarly to zoledronic acid, minodronate, and FDP. Similar hydrogen bonding interactions with the bisphosphonate backbones were seen, as well as an additional hydrogen bond between the dibenzofuran oxygen to Ser71. In the second mode, they found the bisphosphonate moiety to bind the IPP diphosphate site, but the aromatic moiety extended into the GGDPi site. Clearly, longer bisphosphonates exhibited higher potency as GGDPS inhibitors as they experienced enhanced van der Waals and hydrophobic interactions by binding at the GGDPi site. This was also observed by Zhang and coworkers when they investigated the activity of pyridium bisphosphonates on their ability to inhibit both GGDPS and FDPS (PDB: 2ZEU; ref. 66). They noted that longer analogs would sterically clash with residues found at the distal end of the GGDPi binding pocket (Leu42 and Thr177) and would likely show diminished activity. Also, increased potency could be attributed to Mg^{2+} chelation in cases where the bisphosphonate group was bound to the FDP site. The overlaid structure of these inhibitors bound to GGDPS is shown in **Fig. 3B**.

A year later, the same group investigated the activity of 60 bisphosphonates using both crystallography and computational methods (67). Including the known GGDPS inhibitor, digeranyl bisphosphonate (DGBP), a total of seven drug-bound yGGDPS structures were solved (PDB: 2Z4W, 2Z4Y, 2Z4Z, 2Z50, 2Z52, 2Z71, 2Z78). These compounds had varying alkyl chain lengths and substituents to guide SAR investigations. They found the most potent inhibitors to contain long alkyl chains with smaller substituents. When comparing alkyl chain lengths alone, they discovered that BPH-252, which contained six carbons, had better activity than BPH-23 (nine carbons) and BPH-28 (four carbons). Two phosphonate groups were necessary for activity as they saw no activity with a phosphonosulfonate analog. BPH-742 appeared to have the best activity, containing a 10-carbon chain and cationic center. However, their computational studies showed the cationic center was not essential for activity (68, 69). In addition, they also showed that "V-shaped" dialkenyl bisphosphonates and biphenyl-containing inhibitors could simultaneously bind both the FDP and GGDPi isoprene sites. Continued efforts include optimizing these V-shaped compounds for more selective GGDPS inhibition (70–72). Structures containing these inhibitors at the GGDPS active site are overlaid and shown in **Fig. 3C**.

Zhou and coworkers identified a series of geranyl and neryl triazole bisphosphonates as the first of a new family of potent GGDPS inhibitors. These contained a single triazole bisphosphonate group with a 10-carbon alkyl chain. The neryl isomer was almost 40-fold more potent than the geranyl isomer (73, 74). Subsequently, Wills and colleagues generated homoneryl and homogeranyl triazole bisphosphonates containing an 11-carbon alkyl side chain (75). When tested separately, the homoneryl isomer was more potent than the homogeranyl isomer (IC_{50}: 74.9 nmol/L vs. 173.3 nmol/L). When tested as a mixture of isomers, it was discovered that the two isomers interacted synergistically to inhibit the target enzyme. The discovered 3:1 mixture of homogeranyl:homoneryl olefin isomers is currently the most potent

GGDPS inhibitor yet (IC_{50}: 45 nmol/L; refs. 75, 76). Docking studies offered a potential explanation for the synergism as it showed the homoneryl isomer preferentially bound the FDP isoprene site, while the homogeranyl isomer preferentially bound the GGDPi site. The homoneryl isomer interacted with the FDP site at Arg39, Arg84, and Arg85 through hydrogen bonds. The homogeranyl isomer was bound at the GGDPi site, with Lys233, Tyr205, Gln142, Thr170, and Lys169 being important hydrogen bonding partners to the triazole group. For both isomers, hydrophobic interactions were seen between the isoprene side chain and the hydrophobic channels/pockets of GGDPS. Greater GGDPS inhibition was seen in the homogeranyl/-neryl compounds compared with bishomogeranyl/neryl compounds (12-carbon alkyl side chains) (77). Thus, these studies show that both alkyl side chain length and stereochemistry play roles in GGDPS inhibition.

Additional studies worked to improve cellular delivery/uptake by examining the effects of ω and α substitutions. The ω-hydroxyl substitutions on the geranyl/neryl triazole bisphosphonates showed retained but diminished GGDPS inhibitory activity compared with the non-substituted parent compounds. However, the ω-hydroxyl group enabled conjugation to hyaluronic acid (HA) for improved cellular uptake. Indeed, an HA-GGDPS inhibitor conjugate demonstrated enhanced cellular activity compared with the free drug (78). When looking at the effects of α-modifications on activity, Matthiesen and coworkers observed that α-methylation of the geranyl/neryl triazole bisphosphonates had a 5-fold increase in cellular potency compared with the unsubstituted parent. However, α-methylation of the homogeranyl/homoneryl triazole bisphosphonates abrogated the synergism seen with the unmodified compounds (34, 79). Despite the α-methyl homogeranyl/homoneryl triazole bisphosphonates having equivalent activity in enzymatic and cellular assays, preclinical studies revealed differences between the two isomers concerning pharmacokinetic, biodistribution, and toxicity. Further understanding of the impact of the olefin stereochemistry on *in vivo* activity is needed.

Further studies investigated the effects of other substitutions at the α-position. Interestingly, an α-hydroxyl addition could recapitulate similar potency as the α-methylated derivative. This contrasts with the ω-hydroxyl substitution, which showed decreased cellular activity compared with the parent. The study also identified an α-aminomethylene derivative that showed acceptable cellular activity. Both the α-hydroxyl and α-aminomethylene derivatives are of particular interest as they are potentially linkable (80).

In 2018, Lacbay and colleagues reported the activity of novel thienopyrimidine-based bisphosphonates in multiple myeloma cell lines (40). Starting with a thienopyrimidine containing bisphosphonate parent, they found that the carbon position of the added substituents affected hGGDPS selectivity over FDPS. SAR optimization showed that higher hGGDPS selectivity could be attained by extending the side chain, which was achieved by adding a benzamide group to a phenyl-substituted compound. Their lead compound was generated by adding fluorine to the benzamide ring (FV0109, IC_{50}: 0.042 μmol/L), and the structure of FV0109-bound hGGDPS was ultimately solved (PDB: 6C57). The solved structure used the dimeric $hGGDPS^{Y246D}$ mutant. Through the structure, they observed the bisphosphonate group of their lead compound binds between the conserved aspartate-rich motifs (DDXXD) to compete with the FDP diphosphate. The fluorophenyl tail occupied the FDP isoprene site, and the thienopyrimidine core extended into the IPP binding site. Arg73, Gln185, and Lys212 contributed to the stabilization of the charged bisphosphonate. While their structure did not contain any Mg^{2+}, their differential scanning fluorimetry experiments indicated Mg^{2+} was necessary for binding. Solved eukaryotic GGDPS structures are relatively limited, but the structures described here provide valuable insight into inhibitor binding and SAR. Inhibitor-bound hGGDPS structures, including a zolderonate-bound D188Y mutant (65), are overlaid and shown in **Fig. 3D**.

A current limitation of GGDPS inhibitor progress is that studies to date are biased to closely mimic the substrate or product. Fragment-based drug discovery (FBDD) is one way to overcome this (81–83). FBDD is a high throughput drug screening method which uses structural techniques to screen small fragments rather than entire compounds. Once the fragments are identified, they are rationally linked on the basis of the SARs to form a new lead compound. GGDPS is a complex multi-unit enzyme, therefore structure-based methods of identifying new inhibitors seem sensible. As structural techniques continue to evolve, so does the reliability of models and their role in drug screening and optimization. The recent explosion of AlphaFold and structure predicting software have laid the foundation for drug discovery with proteins which have no structural data (84, 85). Furthermore, computational-based techniques such as molecular docking and molecular dynamics continue to improve in both efficiency and accuracy (19, 86). These virtual approaches could serve as robust methods to identify new leads and ways to improve current inhibitors which have remained a key bottleneck in drug discovery (87). The relationship between structure and function continues to be revealed through scientific discovery. By applying these relationships to drug discovery methods, we can truly streamline the process of finding new therapeutics.

Conclusion

The structural knowledge of GGDPS continues to grow, and strategies to design effective GGDPS inhibitors also grow. More literature continues to implicate the role of GGDPS in cancer progression and metastasis. As more direct relationships are elucidated, inhibitor development must be streamlined. Structurally, GGDPS homo-oligomerizes, and the appearance of multiple active forms with different oligomerization states remains puzzling. However, solved hGGDPS structures show two important oligomerization interfaces, the dimer and trimer interfaces. A substantial roadblock is the lack of wild type hGGDPS structures. Notably, no substrate-bound or apo wild type hGGDPS structures exist. Thus, a comprehensive model for molecular simulations and docking studies cannot be made. Furthermore, an accurate look at the hGGDPS substrate binding site remains elusive. Even then, the high sequence identity of hGGDPS and yGGDPS paired with the wealth of yGGDPS structures allowed us to examine the likely substrate/product-binding site of hGGDPS. Two distinct substrate binding sites are seen within GGDPS; one accommodates the smaller IPP substrate while the other binds the larger FDP substrate. The GGDP product occupies two potential sites, one which overlaps with the substrate site and the other which occupies a long hydrophobic channel (the GGDPi site). The coordination of GGDPS with Mg^{2+} not only facilitates the stabilization of the lipophilic substrates but may also play a role in drawing them in. The plethora of inhibitor-bound GGDPS structures allowed us to take a comprehensive look at how different bisphosphonates bind the active site. Through this, we can see that certain binding motifs exist. Bisphosphonates typically occupy the IPP or FDP diphosphate site, and compound side chains occupy either the FDP or GGDPi isoprene site. We also discussed established structure–activity relationships between synthesized bisphosphonates and the enzyme. These relationships suggest the bisphosphonates group is essential for activity and that

alkyl side chain length, stereochemistry, and position of substituent addition all affect potency.

Considerable efforts from a multitude of researchers have contributed much to the GGDPS structural landscape. However, many questions remain unanswered. As structural techniques become more accurate and sophisticated, more insight into the structural properties of GGDPS will be uncovered.

Authors' Disclosures

S.A. Holstein reports grants from NIH during the conduct of the study. No disclosures were reported by the other authors.

Acknowledgments

This research was supported by NIH/NCI R01CA258621 to S.A. Holstein, Department of Education Graduate Assistance in Areas of National Need (GAANN) P200A210032 to G.E.O. Borgstahl, and the NIH/NCI P30CA036727 Eppley Cancer Center Support grant.

Note

Supplementary data for this article are available at Molecular Cancer Therapeutics Online (http://mct.aacrjournals.org/).

Received June 12, 2023; revised August 9, 2023; accepted September 22, 2023; published first September 26, 2023.

References

1. Zhang FL, Casey PJ. Protein prenylation: molecular mechanisms and functional consequences. Annu Rev Biochem 1996;65:241–69.
2. Takai Y, Sasaki T, Matozaki T. Small GTP-binding proteins. Physiol Rev 2001;81:153–208.
3. Tzeng HT, Wang YC. Rab-mediated vesicle trafficking in cancer. J Biomed Sci 2016;23:70.
4. Prieto-Dominguez N, Parnell C, Teng Y. Drugging the small GTPase pathways in cancer treatment: promises and challenges. Cells 2019;8:255.
5. Wang M, Casey PJ. Protein prenylation: unique fats make their mark on biology. Nat Rev Mol Cell Biol 2016;17:110–22.
6. Swan G, Geng J, Park E, Ding Q, Zhou J, Walcott C, et al. A requirement of protein geranylgeranylation for chemokine receptor signaling and Th17 cell function in an animal model of multiple sclerosis. Front Immunol 2021;12:641188.
7. Vogt A, Qian Y, McGuire TF, Hamilton AD, Sebti SM. Protein geranylgeranylation, not farnesylation, is required for the G_1 to S phase transition in mouse fibroblasts. Oncogene 1996;13:1991–9.
8. Kuchay S, Wang H, Marzio A, Jain K, Homer H, Fehrenbacher N, et al. GGTase3 is a newly identified geranylgeranyltransferase targeting a ubiquitin ligase. Nat Struct Mol Biol 2019;26:628–36.
9. Shirakawa R, Goto-Ito S, Goto K, Wakayama S, Kubo H, Sakata N, et al. A SNARE geranylgeranyltransferase essential for the organization of the Golgi apparatus. EMBO J 2020;39:e104120.
10. Marchwicka A, Kaminska D, Monirialamdari M, Blazewska KM, Gendaszewska-Darmach E. Protein prenyltransferases and their inhibitors: structural and functional characterization. Int J Mol Sci 2022;23:5424.
11. Taylor JS, Reid TS, Terry KL, Casey PJ, Beese LS. Structure of mammalian protein geranylgeranyltransferase type-I. EMBO J 2003;22:5963–74.
12. Thoma NH, Iakovenko A, Owen D, Scheidig AS, Waldmann H, Goody RS, et al. Phosphoisoprenoid binding specificity of geranylgeranyltransferase type II. Biochemistry 2000;39:12043–52.
13. Roth AF, Davis NG. Geranylgeranyl generosity: a new prenyl-transferase gives a fat to a SNARE protein. EMBO J 2020;39:e104744.
14. Reid TS, Terry KL, Casey PJ, Beese LS. Crystallographic analysis of CaaX prenyltransferases complexed with substrates defines rules of protein substrate selectivity. J Mol Biol 2004;343:417–33.
15. Muehlebach ME, Holstein SA. Geranylgeranyl diphosphate synthase: role in human health, disease and potential therapeutic target. Clin Transl Med 2023;13:e1167.
16. Shah S, Brock EJ, Ji K, Mattingly RR. Ras and Rap1: A tale of two GTPases. Semin Cancer Biol 2019;54:29–39.
17. Crosas-Molist E, Samain R, Kohlhammer L, Orgaz JL, George SL, Maiques O, et al. Rho GTPase signaling in cancer progression and dissemination. Physiol Rev 2022;102:455–510.
18. Kazanietz MG, Caloca MJ. The Rac GTPase in cancer: from old concepts to new paradigms. Cancer Res 2017;77:5445–51.
19. Batool M, Ahmad B, Choi S. A structure-based drug discovery paradigm. Int J Mol Sci 2019;20:2783.
20. Aplin C, Milano SK, Zielinski KA, Pollack L, Cerione RA. Evolving experimental techniques for structure-based drug design. J Phys Chem B 2022;126:6599–607.
21. Dudakovic A, Tong H, Hohl RJ. Geranylgeranyl diphosphate depletion inhibits breast cancer cell migration. Invest New Drugs 2011;29:912–20.
22. Agabiti SS, Liang Y, Wiemer AJ. Molecular mechanisms linking geranylgeranyl diphosphate synthase to cell survival and proliferation. Mol Membr Biol 2016;33:1–11.
23. Agabiti SS, Li J, Wiemer AJ. Geranylgeranyl diphosphate synthase inhibition induces apoptosis that is dependent upon GGPP depletion, ERK phosphorylation, and caspase activation. Cell Death Dis 2017;8:e2678.
24. Agabiti SS, Li J, Dong W, Poe MM, Wiemer AJ. Regulation of the Notch-ATM-abl axis by geranylgeranyl diphosphate synthase inhibition. Cell Death Dis 2019;10:733.
25. Holstein SA, Tong H, Hohl RJ. Differential activities of thalidomide and isoprenoid biosynthetic pathway inhibitors in multiple myeloma cells. Leuk Res 2010;34:344–51.
26. Dudakovic A, Wiemer AJ, Lamb KM, Vonnahme LA, Dietz SE, Hohl RJ. Inhibition of geranylgeranyl diphosphate synthase induces apoptosis through multiple mechanisms and displays synergy with inhibition of other isoprenoid biosynthetic enzymes. J Pharmacol Exp Ther 2008;324:1028–36.
27. Wasko BM, Dudakovic A, Hohl RJ. Bisphosphonates induce autophagy by depleting geranylgeranyl diphosphate. J Pharmacol Exp Ther 2011;337:540–6.
28. Dykstra KM, Allen C, Born EJ, Tong H, Holstein SA. Mechanisms for autophagy modulation by isoprenoid biosynthetic pathway inhibitors in multiple myeloma cells. Oncotarget 2015;6:41535–49.
29. Haney SL, Feng D, Chhonker YS, Varney ML, Williams JT, Smith LM, et al. Evaluation of geranylgeranyl diphosphate synthase inhibition as a novel strategy for the treatment of osteosarcoma and Ewing sarcoma. Drug Dev Res 2023;84:62–74.
30. Ullah N, Mansha M, Casey PJ. Protein Geranylgeranyltransferase type 1 as a target in cancer. Curr Cancer Drug Targets 2016;16:563–71.
31. Obeng EA, Carlson LM, Gutman DM, Harrington WJ Jr., Lee KP, Boise LH. Proteasome inhibitors induce a terminal unfolded protein response in multiple myeloma cells. Blood 2006;107:4907–16.
32. Holstein SA, Hohl RJ. Isoprenoid biosynthetic pathway inhibition disrupts monoclonal protein secretion and induces the unfolded protein response pathway in multiple myeloma cells. Leuk Res 2011;35:551–9.
33. Born EJ, Hartman SV, Holstein SA. Targeting HSP90 and monoclonal protein trafficking modulates the unfolded protein response, chaperone regulation and apoptosis in myeloma cells. Blood Cancer J 2013;3:e167.
34. Haney SL, Chhonker YS, Varney ML, Talmon G, Smith LM, Murry DJ, et al. *In vivo* evaluation of isoprenoid triazole bisphosphonate inhibitors of geranylgeranyl diphosphate synthase: impact of olefin stereochemistry on toxicity and biodistribution. J Pharmacol Exp Ther 2019;371:327–38.
35. Haney SL, Varney ML, Chhonker YS, Shin S, Mehla K, Crawford AJ, et al. Inhibition of geranylgeranyl diphosphate synthase is a novel therapeutic strategy for pancreatic ductal adenocarcinoma. Oncogene 2019;38:5308–20.
36. Reilly JE, Neighbors JD, Hohl RJ. Targeting protein geranylgeranylation slows tumor development in a murine model of prostate cancer metastasis. Cancer Biol Ther 2017;18:872–82.
37. Reilly JE, Neighbors JD, Tong H, Henry MD, Hohl RJ. Targeting geranylgeranylation reduces adrenal gland tumor burden in a murine model of prostate cancer metastasis. Clin Exp Metastasis 2015;32:555–66.
38. Haney SL, Varney ML, Chhonker Y, Talmon G, Smith LM, Murry DJ, et al. *In vivo* evaluation of combination therapy targeting the isoprenoid biosynthetic pathway. Pharmacol Res 2021;167:105528.
39. Haney SL, Varney ML, Williams JT, Smith LM, Talmon G, Holstein SA. Geranylgeranyl diphosphate synthase inhibitor and proteasome inhibitor combination therapy in multiple myeloma. Exp Hematol Oncol 2022;11:5.
40. Lacbay CM, Waller DD, Park J, Gomez Palou M, Vincent F, Huang XF, et al. Unraveling the prenylation-cancer paradox in multiple myeloma with novel

Geranylgeranyl Pyrophosphate Synthase (GGPPS) inhibitors. J Med Chem 2018; 61:6904–17.
41. Wang X, Xu W, Zhan P, Xu T, Jin J, Miu Y, et al. Overexpression of geranylgeranyl diphosphate synthase contributes to tumor metastasis and correlates with poor prognosis of lung adenocarcinoma. J Cell Mol Med 2018;22:2177–89.
42. Yu DC, Liu J, Chen J, Shao JJ, Shen X, Xia HG, et al. GGPPS1 predicts the biological character of hepatocellular carcinoma in patients with cirrhosis. BMC Cancer 2014;14:248.
43. Sagami H, Korenaga T, Ogura K, Steiger A, Pyun HJ, Coates RM. Studies on geranylgeranyl diphosphate synthase from rat liver: specific inhibition by 3-azageranylgeranyl diphosphate. Arch Biochem Biophys 1992;297:314–20.
44. Sagami H, Morita Y, Ogura K. Purification and properties of geranylgeranyldiphosphate synthase from bovine brain. J Biol Chem 1994;269:20561–6.
45. Chang TH, Guo RT, Ko TP, Wang AH, Liang PH. Crystal structure of type-III geranylgeranyl pyrophosphate synthase from Saccharomyces cerevisiae and the mechanism of product chain length determination. J Biol Chem 2006;281: 14991–5000.
46. Guo RT, Cao R, Liang PH, Ko TP, Chang TH, Hudock MP, et al. Bisphosphonates target multiple sites in both cis- and trans-prenyltransferases. Proc Natl Acad Sci USA 2007;104:10022–7.
47. Kavanagh KL, Dunford JE, Bunkoczi G, Russell RGG, Oppermann U. The crystal structure of human geranylgeranyl pyrophosphate synthase reveals a novel hexameric arrangement and inhibitory product binding. J Biol Chem 2006; 281:22004–12.
48. Wang C, Chen Q, Fan D, Li J, Wang G, Zhang P. Structural analyses of short-chain prenyltransferases identify an evolutionarily conserved GFPPS clade in brassicaceae plants. Mol Plant 2016;9:195–204.
49. Wallrapp FH, Pan JJ, Ramamoorthy G, Almonacid DE, Hillerich BS, Seidel R, et al. Prediction of function for the polyprenyl transferase subgroup in the isoprenoid synthase superfamily. Proc Natl Acad Sci USA 2013;110:E1196–202.
50. Zhou F, Wang CY, Gutensohn M, Jiang L, Zhang P, Zhang D, et al. A recruiting protein of geranylgeranyl diphosphate synthase controls metabolic flux toward chlorophyll biosynthesis in rice. Proc Natl Acad Sci USA 2017;114:6866–71.
51. Chang TH, Hsieh FL, Ko TP, Teng KH, Liang PH, Wang AH. Structure of a heterotetrameric geranyl pyrophosphate synthase from mint (Mentha piperita) reveals intersubunit regulation. Plant Cell 2010;22:454–67.
52. Kim S, Kim EJ, Park JB, Kim SW, Kim KJ. Crystal structure of geranylgeranyl pyrophosphate synthase (crtE) from Nonlabens dokdonensis DSW-6. Biochem Biophys Res Commun 2019;518:479–85.
53. Kuzuguchi T, Morita Y, Sagami I, Sagami H, Ogura K. Human geranylgeranyl diphosphate synthase. cDNA cloning and expression. J Biol Chem 1999;274: 5888–94.
54. Miyagi Y, Matsumura Y, Sagami H. Human geranylgeranyl diphosphate synthase is an octamer in solution. J Biochem 2007;142:377–81.
55. Schrodinger LLC. The PyMOL Molecular Graphics System, Version 1.8. 2015.
56. Lisnyansky M, Yariv E, Segal O, Marom M, Loewenstein A, Ben-Tal N, et al. Metal coordination is crucial for geranylgeranyl diphosphate synthase-bisphosphonate interactions: a crystallographic and computational analysis. Mol Pharmacol 2019;96:580–8.
57. Jumper J, Evans R, Pritzel A, Green T, Figurnov M, Ronneberger O, et al. Highly accurate protein structure prediction with AlphaFold. Nature 2021; 596:583–9.
58. Waterhouse AM, Procter JB, Martin DM, Clamp M, Barton GJ. Jalview Version 2–a multiple sequence alignment editor and analysis workbench. Bioinformatics 2009;25:1189–91.
59. Kavanagh KL, Guo K, Dunford JE, Wu X, Knapp S, Ebetino FH, et al. The molecular mechanism of nitrogen-containing bisphosphonates as antiosteoporosis drugs. Proc Natl Acad Sci USA 2006;103:7829–34.
60. Ramsay RR, Tipton KF. Assessment of enzyme inhibition: a review with examples from the development of monoamine oxidase and cholinesterase inhibitory drugs. Molecules 2017;22:1192.
61. Hopkins AL, Groom CR. The druggable genome. Nat Rev Drug Discov 2002;1: 727–30.
62. Poulter CD, Satterwhite DM. Mechanism of the prenyl-transfer reaction. Studies with (E)- and (Z)-3-trifluoromethyl-2-buten-1-yl pyrophosphate. Biochemistry 1977;16:5470–8.
63. Poulter CD, Argyle JC, Mash EA. Farnesyl pyrophosphate synthetase. Mechanistic studies of the 1'-4 coupling reaction with 2-fluorogeranyl pyrophosphate. J Biol Chem 1978;253:7227–33.
64. Szabo CM, Matsumura Y, Fukura S, Martin MB, Sanders JM, Sengupta S, et al. Inhibition of geranylgeranyl diphosphate synthase by bisphosphonates and diphosphates: a potential route to new bone antiresorption and antiparasitic agents. J Med Chem 2002;45:2185–96.
65. Lisnyansky M, Kapelushnik N, Ben-Bassat A, Marom M, Loewenstein A, Khananshvili D, et al. Reduced activity of geranylgeranyl diphosphate synthase mutant is involved in bisphosphonate-induced atypical fractures. Mol Pharmacol 2018;94:1391–400.
66. Zhang Y, Cao R, Yin F, Hudock MP, Guo RT, Krysiak K, et al. Lipophilic bisphosphonates as dual farnesyl/geranylgeranyl diphosphate synthase inhibitors: an X-ray and NMR investigation. J Am Chem Soc 2009;131:5153–62.
67. K-M Chen C, Hudock MP, Zhang Y, Guo RT, Cao R, No JH, et al. Inhibition of geranylgeranyl diphosphate synthase by bisphosphonates: a crystallographic and computational investigation. J Med Chem 2008;51:5594–607.
68. Martin MB, Arnold W, Heath HT 3rd, Urbina JA, Oldfield E. Nitrogen-containing bisphosphonates as carbocation transition state analogs for isoprenoid biosynthesis. Biochem Biophys Res Commun 1999;263:754–8.
69. Sanders JM, Gomez AO, Mao J, Meints GA, Van Brussel EM, Burzynska A, et al. 3-D QSAR investigations of the inhibition of Leishmania major farnesyl pyrophosphate synthase by bisphosphonates. J Med Chem 2003;46:5171–83.
70. Barney RJ, Wasko BM, Dudakovic A, Hohl RJ, Wiemer DF. Synthesis and biological evaluation of a series of aromatic bisphosphonates. Bioorg Med Chem 2010;18:7212–20.
71. Foust BJ, Allen C, Holstein SA, Wiemer DF. A new motif for inhibitors of geranylgeranyl diphosphate synthase. Bioorg Med Chem 2016;24:3734–41.
72. Zhou X, Reilly JE, Loerch KA, Hohl RJ, Wiemer DF. Synthesis of isoprenoid bisphosphonate ethers through C-P bond formations: Potential inhibitors of geranylgeranyl diphosphate synthase. Beilstein J Org Chem 2014;10:1645–50.
73. Zhou X, Ferree SD, Wills VS, Born EJ, Tong H, Wiemer DF, et al. Geranyl and neryl triazole bisphosphonates as inhibitors of geranylgeranyl diphosphate synthase. Bioorg Med Chem 2014;22:2791–8.
74. Zhou X, Hartman SV, Born EJ, Smits JP, Holstein SA, Wiemer DF. Triazole-based inhibitors of geranylgeranyltransferase II. Bioorg Med Chem Lett 2013;23: 764–6.
75. Allen C, Kortagere S, Tong H, Matthiesen RA, Metzger JI, Wiemer DF, et al. Olefin Isomers of a triazole bisphosphonate synergistically inhibit geranylgeranyl diphosphate synthase. Mol Pharmacol 2017;91:229–36.
76. Wills VS, Allen C, Holstein SA, Wiemer DF. Potent triazole bisphosphonate inhibitor of geranylgeranyl diphosphate synthase. ACS Med Chem Lett 2015;6: 1195–8.
77. Wills VS, Metzger JI, Allen C, Varney ML, Wiemer DF, Holstein SA. Bishomoisoprenoid triazole bisphosphonates as inhibitors of geranylgeranyl diphosphate synthase. Bioorg Med Chem 2017;25:2437–44.
78. Bhuiyan NH, Varney ML, Bhattacharya DS, Payne WM, Mohs AM, Holstein SA, et al. omega-Hydroxy isoprenoid bisphosphonates as linkable GGDPS inhibitors. Bioorg Med Chem Lett 2019;29:126633.
79. Matthiesen RA, Varney ML, Xu PC, Rier AS, Wiemer DF, Holstein SA. alpha-Methylation enhances the potency of isoprenoid triazole bisphosphonates as geranylgeranyl diphosphate synthase inhibitors. Bioorg Med Chem 2018;26: 376–85.
80. Fairweather AER, Goetz DB, Schroeder CM, Bhuiyan NH, Varney ML, Wiemer DF, et al. Impact of alpha-modifications on the activity of triazole bisphosphonates as geranylgeranyl diphosphate synthase inhibitors. Bioorg Med Chem 2021;44:116307.
81. Rees DC, Congreve M, Murray CW, Carr R. Fragment-based lead discovery. Nat Rev Drug Discov 2004;3:660–72.
82. Erlanson DA. Introduction to fragment-based drug discovery. Top Curr Chem 2012;317:1–32.
83. Kirsch P, Hartman AM, Hirsch AKH, Empting M. Concepts and core principles of fragment-based drug design. Molecules 2019;24:4309.
84. Kim Y, Kim S. Target discovery using deep learning-based molecular docking and predicted protein structures with alphafold for novel antipsychotics. Psychiatry Investig 2023;20:504–14.
85. Borkakoti N, Thornton JM. AlphaFold2 protein structure prediction: Implications for drug discovery. Curr Opin Struct Biol 2023;78:102526.
86. Naqvi AAT, Mohammad T, Hasan GM, Hassan MI. Advancements in docking and molecular dynamics simulations towards ligand-receptor interactions and structure-function relationships. Curr Top Med Chem 2018;18:1755–68.
87. Dove A. Drug screening–beyond the bottleneck. Nat Biotechnol 1999;17:859–63.